Aquarius CAP Algorithm and Data User Guide

Version: 2.0

Simon Yueh

Jet Propulsion Laboratory

California Institute of Technology

Date: February 20, 2013

Contributors

The Aquarius geophysical model functions for the CAP algorithm were developed by Dr. Wenqing Tang; the operational setup and processing of the CAP algorithm was completed by Dr. Alex Fore; the setup of data portal and data transfer was performed by Mrs. Akiko Hayashi.

Document Change Log

Date	*Page Numbers*	Version	Changes/Comments
February 20, 2013	Page 8	2.0	Updated the cost function by adding two additional terms to constrain the wind speed and direction retrieval
February 20, 2013	Page 11	2.0	Add 10 to the flag to indicate possible rain contamination
February 20, 2013	Pages 5 and 6	2.0	Include the significant wave height as a modeling parameter for radar backscatter and excess emissivity

Contents

I. PURPOSE

This document provides an overview of the Combined Active-Passive (CAP) Algorithm for the sea surface roughness correction to enable the retrieval of sea surface salinity, wind speed and direction from Aquarius data without the need to use ancillary NCEP winds for correction. The results from the CAP algorithm are output to files in HDF5 format. This document describes the datasets in the files and their format.

II. INTRODUCTION

The measurement principle for salinity remote sensing is based on the response of the L-band (1.413 GHz) sea surface brightness temperatures (T_B) to sea surface salinity [1]. The influence of wind speed on L-band T_B has been shown to be about 0.2 to 0.3 K for one m.s^{-1} change in wind speed by many field studies [2-7]. To achieve the required 0.2 practical salinity unit (psu) accuracy, the impact of sea surface roughness (e.g. wind-generated ripples, foam, and swells) on the observed brightness temperature has to be accurately corrected, ideally to better than one tenth of a degree Kelvin.

The Aquarius radiometer and scatterometer have been fully operating since August 25, 2011. Other than the interruptions caused by a few spacecraft maneuvers, the data acquisition has been continuous. The Aquarius instrument has three antenna beams, operating at about 29, 38 and 46 degrees [8]. Each antenna beam has one radiometer (1.413 GHz), which can acquire the first three Stokes parameters of microwave radiation. The antenna feeds are shared with the scatterometer (1.26 GHz), which acquire the normalized radar cross sections (σ_0) for co- and cross-polarizations, including VV, HH, VH and HV polarizations.

The Aquarius radiometers make partial polarimetric measurements for the first three Stokes parameters, I, Q, and U [9]. I and Q correspond to the sum and difference of the vertically polarized brightness temperature (T_{BV}) and horizontally polarized brightness temperature (T_{BH}). T_{BV} and T_{BH} are measures of the power of the vertically polarized electrical field (E_V) and horizontally polarized electric field (E_H), while the third and fourth Stokes parameters (U and V) signify the correlation between E_V and E_H:

$$\begin{bmatrix} I \\ Q \\ U \\ V \end{bmatrix} = \begin{bmatrix} T_{BV} + T_{BH} \\ T_{BV} - T_{BH} \\ U \\ V \end{bmatrix} \propto \begin{bmatrix} \left\langle |E_v|^2 \right\rangle + \left\langle |E_H|^2 \right\rangle \\ \left\langle |E_v|^2 \right\rangle - \left\langle |E_H|^2 \right\rangle \\ 2\,\mathrm{Re}\left\langle E_v E_H^* \right\rangle \\ 2\,\mathrm{Im}\left\langle E_v E_H^* \right\rangle \end{bmatrix} \quad \textbf{(1)}$$

The angular brackets denote the ensemble average of the enclosed quantities. Aquarius does not measure the fourth Stokes V.

The matchup data using either SSM/I or NCEP wind for binning have been used to develop the geophysical model functions (GMF) for Aquarius [12], which relate the microwave backscatter or excess surface emissivity to the wind speed (w) and direction (ϕ). In addition, we include the NOAA WaveWatch-III Significant Wave Height (SWH) to develop the GMF and as ancillary for retrieval. We use the following cosine series for the modeling of radar data:

$$\sigma_{VV}(w,\phi,SWH) = A_{0VV}(w,SWH)[1 + A_{1VV}(w)\cos\phi + A_{2VV}(w)\cos 2\phi] \quad \textbf{(2)}$$

$$\sigma_{HH}(w,\phi,SWH) = A_{0HH}(w,SWH)[1 + A_{1HH}(w)\cos\phi + A_{2HH}(w)\cos 2\phi] \quad \textbf{(3)}$$

Here σ_{VV} and σ_{HH} are the normalized radar backscatter cross-sections for V-transmit/V-receive and H-transmit/H-receive, respectively. The modeling coefficients in Eqs. (2) and (3) are illustrated in [12].

For the radiometer model function, we use the following expressions to characterize the dependence of excess surface emissivity on wind speed, wind direction and SWH:

$$\Delta e_V(w,\phi,SWH) = e_{V0}(w,SWH) + e_{V1}(w)\cos\phi + e_{V2}(w)\cos 2\phi \quad \textbf{(3)}$$

$$\Delta e_H(w,\phi,SWH) = e_{H0}(w,SWH) + e_{H1}(w)\cos\phi + e_{H2}(w)\cos 2\phi \quad \textbf{(4)}$$

$$U(w,\phi) = U_1(w)\sin\phi + U_2(w)\sin 2\phi \quad \textbf{(5)}$$

The third Stokes parameter for the L-band frequency is modeled by the sine function of the wind direction. The modeling coefficients for Δe_V and Δe_H are illustrated in [12].

Given the GMF for excess surface emissivity, following are the complete descriptions of the radiometer model function, which relates the brightness temperatures to surface salinity (SSS), SST, wind speed, wind direction and SWH:

$$T_{BV}(SSS,SST,w,\phi,SWH) = T_{BVflat}(SSS,SST) + SST\cdot\Delta e_{BV}(w,\phi,SWH) \quad \textbf{(6)}$$

$$T_{BH}(SSS,SST,w,\phi,SWH) = T_{BHflat}(SSS,SST) + SST\cdot\Delta e_{BH}(w,\phi,SWH) \quad \textbf{(7)}$$

$$U(SSS,SST,w,\phi) = U_1(w)\sin\phi + U_2(w)\sin 2\phi \quad \textbf{(8)}$$

T_{Bflat} is the brightness temperature for flat water surfaces computed using the water dielectric constant model [10] for given Reynolds SST and SSS. The subscript "p" stands for the polarization.

III. Overview of CAP algorithm

The current approach for Aquarius salinity retrieval algorithm requires the use of ancillary ocean surface wind direction from the National Centers for Environmental Prediction (NCEP) to make corrections to ocean brightness temperatures. Any errors in the NCEP analyses, particularly for high winds or near the front, as well as temporal mismatch with the Aquarius sampling may not allow the directional effects to be accurately removed. To remove the dependence on the NCEP wind direction for retrieval, the Combined Active-Passive (CAP) algorithm [11, 12] was developed to retrieve the salinity and wind without the need to use the NCEP winds for corrections.

The CAP algorithm simultaneously retrieves the salinity, wind speed and direction by minimizing the sum of squared differences between model and observations. After testing the CAP algorithm against the Aquarius data, we find that the following Least Square Error (LSE) performs very well for the Aquarius version 1.3 data

$$F_{cap}(SSS,w,\phi)=\frac{(I-I_m)^2}{2\Delta T^2}+\frac{(\sqrt{Q^2+U^2}-\sqrt{Q_m^2+U_m^2})^2}{2\Delta T^2}+\frac{(\sigma_{VV}-\sigma_{VVm})^2}{{k_{pc}}^2{\sigma_{VV}}^2}+\frac{(\sigma_{HH}-\sigma_{HHm})^2}{{k_{pc}}^2{\sigma_{HH}}^2} \quad \textbf{(9)}$$

In the above equation, I, Q, U, σ_{VV}, and σ_{HH}, represent measurements after Faraday rotation correction, while the quantities with the subscript 'm' correspond to the model functions. The difference between data and model is weighted by the expected uncertainty of measurements. For radiometer data, the minimum uncertainty is the Noise Equivalent Delta T (ΔT). The precision of radar data is limited by the expected signal detection error (k_{pc}). For Aquarius, ΔT is about 0.1 K, and k_{pc} is about 0.01.

The first Stokes parameter ($I=T_{BV}+T_{BH}$) represents the total power of the microwave emission, and is not changed by any polarization rotation. The second Stokes parameter (Q) is influenced by the Faraday rotation, just like the third Stokes parameter (U), but the sum of the squares of Q and U is another invariant quantity under Faraday rotation:

$$I_{QU}=\sqrt{Q^2+U^2} \quad \textbf{(10)}$$

The invariance of I_{QU} under Faraday rotation can be easily shown by using Eqs. (9) and (10) in [13].

Based on the characteristics of the scatterometer GMF derived from more than one year of matchup data, we find that the radar backscatter, particularly for vertical polarization, has significantly reduced sensitivity to wind speed at crosswind direction. The result is that the retrieved wind speed and consequently SSS have larger errors at or near the crosswind direction. In addition, the wind direction dependence of radar backscatter is quite small at low winds; therefore, the retrieved wind direction has a large (> 20 degrees) random error below 8 m s^{-1} wind speeds. For Version 2.0 retrieval, we include the NCEP wind speed and direction as a priori by adding two more terms in the cost function for CAP:

$$F_a=\frac{(w-w_{NCEP})^2}{\Delta w^2}+\frac{\sin^2[(\phi-\phi_{NCEP})/2]}{\delta^2} \quad \textbf{(11)}$$

The weighting coefficients are Δw=1.5 and δ=0.2. The choice of these two values is justified by comparison with the retrieval errors estimated for the CAP product. Using the triple collocation analysis of SSM/I, ECMWF, and CAP, we find that the CAP wind speed error is about 0.7 m s^{-1}, which is a factor of two smaller than 1.5. For directional constraint, δ=0.2 corresponds to about 23 degrees in direction, which is more than two times of the root-mean-square-difference (RMSD) between CAP and NCEP wind directions above 10 m s^{-1}. Therefore, the selected values for the weighting of a priori have small impact on the CAP retrievals where the performance is expected to be excellent, but will mitigate the weakness of the retrievals when the GMF has a reduced sensitivity to the quantity of interest.

$$F_{cap+}(SSS,w,\phi)=F_{cap}(SSS,w,\phi)+F_a \quad \textbf{(12)}$$

For the Aquarius data, we applied the conjugate gradient technique using a modified Levenberg-Marquardt algorithm [14] to find the local minima of F_{cap+}. There are in general four local minima (ambiguous solutions). This is due to the expansion of the model function for wind direction by including up to the second harmonics of the cosine series. For each given wind speed solution, there will in general be four direction solutions, except when the relative wind direction is along upwind, or downwind or crosswind. This can be easily understood by considering the special case when the A_1 coefficients are zero in the model functions. If the first harmonic coefficient A_1 is zero, these four solutions, corresponding to the inversion of $\cos 2\phi$, are ϕ, $-\phi$, $\phi+180^o$ and $180^o-\phi$. If A_1 and e_{B1} are small, then the third and fourth solutions will shift slightly away from $\pm\phi+180^o$. Note that because the cosine series are even functions, the solution pair, $\pm\phi$, will produce identical values for model functions, and consequently lead to the same SSS and wind speed solutions. The same is true for the $\pm\phi+180^o$ solution pair.

A nominal technique developed for the current or past spaceborne wind scatterometer and radiometer missions is the use of numerical weather analysis, such as NCEP or European Center for Medium Range Forecasts (ECMWF), or special wind features to assist the selection of solutions [15]. For salinity and wind speed retrievals, the discrimination of ambiguities is a less challenging issue than ocean wind scatterometers or radiometers because what is needed is to separate the four solutions into two pairs, $\pm\phi$ and $\pm\phi+180^o$, which are separated by about 180 degrees. As previously discussed, each pair will have the same SSS and wind speed values. In our analysis, we use the numerical wind analyses to select the solution by selecting the solution with the closest wind direction to NCEP.

We have validated the accuracy of retrieval using the CAP algorithm for simultaneous wind and salinity retrieval. The retrieved wind speed has very good agreement with the SSMI/S and NCEP wind products (Fig. 1). The directional accuracy also appears very good at above 10 m.s^{-1} wind speeds (Fig. 2). The triple collocation analysis using the SSMI/S, ECMWF and CAP as triplets [16, 17] suggests that the Aquarius CAP wind speed is highly accurate [12], about 0.7 m.s^{-1} in random errors, comparable to SSM/I's.

TABLE 1. ESTIMATED RMSE FOR SSMI/S, ECMWF AND CAP WIND SPEEDS USING TRIPLE COLLOCATIONS.

	SSMI/S	ECMWF	CAP
RMSE wind speed (m/s)	0.714	0.828	0.700

The equivalent GMF modeling error is about 0.12 K, 0.12 K, 0.24 K for beams 1, 2, and 3, respectively, for vertical polarization, close to the desired accuracy for Aquarius. Figs. 1-3 indicate the comparison of Aquarius CAP retrievals with the SSM/I wind speed, NCEP direction and HYCOM SSS. The corresponding CAP salinity error is about 0.5 psu for warm water to 1 psu for cold water for each satellite pass.

The mean and standard deviation of the differences between the CAP and HYCOM SSS for gridded monthly average are illustrated in the right panles in Figs. 3 and 4. The corresponding bias and standard deviation plots for the standard Aquarius V1.3.9 (essentially same as that for

V2.0) are illustrated in the left panels. The CAP bias and standard deviation are smaller than those of the standard V2.0 product over a broader range of wind speed, SST and SWH space. The CAP retrievals appear to have better accuracy at lower SST, higher SWH and higher wind speed.

Figures 5 and 6 illsutrate the bias and standard deviation of monthly averaged CAP SSS with respect to HYCOM on 1 degree latitude and longitude grids. The performance of the standard Aquarius L2 products is illustrated in the left panels for comparison. CAP clearly is superior at mid and high latitudes.

We average the bias and standard deviation of the results plotted in Fig. 5 and 6 over every 10-degree latitude bands. Figure 7 shows that the RMSD between CAP and HYCOM is essentially smaller than 0.25 between +/- 40 degree latitudes. If we assume 0.17 psu error in the HYCOM, the accuracy of CAP would be in the range of 0.1 to 0.2 psu within this latitude range.

IV. CAP HDF DATA AND FORMAT

The Aquarius CAP L2 files contain the CAP algorithm outputs and a few datasets in the Aquarius L2 data files.

A. File name convention

The file names are similar to the Aquarius L2 files. The first part of the file name is the same as that in the Aquarius L2 files. We added the extension '.cap' to it.

For example, Q2012001012500.L2_SCI_V2.0.cap, is the file for the data pass started at 01:25:00 UT on day 1, 2012. "L2_SCI_V2.0" indicates the version of Aquarius L2 files used for the CAP processing.

B. Description of datasets in HDF

The datasets in the HDF5 files are part of the root file, not in a "Aquarius Data" group. Each dataset has 4083 blocks for 3 antenna beams.

1) CAP outputs

The CAP data and critical time and location data sets are outlined below.

Dataset	Size (Block, Beam)	Format	Unit	Valid range	Description
Sec	Dataset {4083, 3}	double float	Seconds	0.d0 to 86399.999999d0	Block time in seconds of day
beam_clat	Dataset {4083, 3}	float	Degree	-90 to 90	Latitude of footprint
beam_clon	Dataset {4083, 3}	float	Degrees	-180 to 180	Longitude of footprint
SSS_cap	Dataset	float	Psu	0 to 50	SSS from the CAP

	{4083, 3}				algorithm
SSS_cap_v	Dataset {4083, 3}	float	Psu	0 to 50	SSS retrieved from the V-pol TB using the scat_wind_speed for excess surface emissivity correction
wind_speed_cap	Dataset {4083, 3}	float	Meters per sec	Greater than 0	Wind speed retrieved from the CAP algorithm
wind_dir_cap	Dataset {4083, 3}	float	Degrees	-180 to 180	Wind direction retrieved from the CAP algorithm
cap_flag	Dataset {4083, 3}	H5T_NATIVE_UCHAR		0 to 4 and 10 to 14	Flag for CAP retrieval
scat_wind_speed	Dataset {4083, 3}	float	Meters per sec	Greater than 0	Wind speed retrieved from the Aquarius scatterometer data using the NCEP wind direction as ancillary information

wind_dir_cap is the wind direction retrieved from the Aquarius data, and is the direction from with respect to the north in clockwise direction. Its error is less than 20 degrees RMS at greater than 12 m/s wind speeds for beam 1 and 10 m/s for beams 2 and 3.

cap_flag: The flag for CAP algorithm retrieval with the values of 0, 1, and 2 for valid SSS retrieval and 3 and 4 for invalid SSS retrieval. If the matchup rain rate (RR) from SSMIS or WindSat is greater than zero, we add 10 to the flag to indicate possible rain contamination.

- 0 for abs(wind_speed_cap-anc_wind_speed) <15 m/s
- 1 for abs(wind_speed_cap-anc_wind_speed) <30 m/s
- 2 for abs(wind_speed_cap-anc_wind_speed) >30 m/s
- 3 for wind_speed_cap <0 or sss_cap < 0 or sss_cap > 50
- 4 for no retrieval
- 10 for abs(wind_speed_cap-anc_wind_speed) <15 m/s and RR>0
- 11 for abs(wind_speed_cap-anc_wind_speed) <30 m/s and RR>0
- 12 for abs(wind_speed_cap-anc_wind_speed) >30 m/s and RR>0
- 13 for wind_speed_cap <0 or sss_cap < 0 or sss_cap > 50 and RR>0

The performance comparison illustrated in Fig. 3 has been using cal_flag from 0 to 2.

2) Carryover from Aquarius L2 files

The following are datasets carried over from the Aquarius L2 files. They are included for ease of comparison with the CAP products.

Dataset	Size (Block, Beam)	Unit	Description

SSS	Dataset {4083, 3}	Psu	SSS in the Aquarius L2 files
anc_SSS	Dataset {4083, 3}	Psu	Ancillary (HYCOM) SSS in the Aquarius L2 files
anc_surface_temp	Dataset {4083, 3}	Kelvin	SST in the Aquarius L2 files
anc_wind_speed	Dataset {4083, 3}	Meters per sec	Ancillary (NCEP) wind speed in the Aquarius L2 files
anc_wind_dir	Dataset {4083, 3}	Degrees	Ancillary wind direction (NCEP) in the Aquarius L2 files
scat_land_frac	Dataset {4083, 3}		Scatteroemter land fraction in the Aquarius L2 files (unitless between 0 and 1)
scat_ice_frac	Dataset {4083, 3}		Scatteroemter ice fraction in the Aquarius L2 files (unitless between 0 and 1)
land_frac	Dataset {4083, 3}		Radiometer land fraction in the Aquarius L2 files (unitless between 0 and 1)
ice_frac	Dataset {4083, 3}		Radioemter ice fraction in the Aquarius L2 files (unitless between 0 and 1)

V. REFERENCES

[1] Yueh, S. H., R. West, W. J. Wilson, F. K. Li, E. G. Njoku, and Y. Rahmat-Samii, Error sources and feasibility for microwave remote sensing of ocean surface salinity, IEEE Trans. Geosci. Remote Sensing, 39, 1049-1060, 2001.

[2] J. P. Hollinger, "Passive microwave measurements of sea surface roughness," *IEEE Trans. Geosci. Electron.*, vol. GE-9, pp. 165–169, July 1971.

[3] Camps A., Font J., Vall-Llossera M, Gabarro C, Corbella I, Duffo N, Torres F, Blanch S, Aguasca A, Villarino R, Enrique L, Miranda JJ, Arenas JJ, Juliaa A, Etcheto J, Caselles V, Weill A, Boutin J, Contardo S, Niclos R, Rivas R, Reising SC, Wursteisen P, Berger M, and Martin-Neira M, "The WISE 2000 and 2001 field experiments in support of the SMOS mission: Sea surface L-band brightness temperature observations and their application to sea surface salinity retrieval," IEEE Trans. Geoscience and Remote Sensing, vol. 42, no. 4, pp. 804-823, April 2004.

[4] J. Etcheto, E. P. Dinnat, J. Boutin, A. Camps, J. Miller, Stephanie, J. Wesson, J. Font, and D. Long, "Wind speed effect on L-band brightness temperature inferred from EuroSTARRS and WISE 2001 field experiments." Vol. 42, no. 10, pp. 2206-2213, October 2004.

[5] C. Gabarro, J. Font, A. Camps, M. Vall-Llossera, and A. Julia, "A new empirical model of sea surface microwave emissivity for salinity remote sensing," Geophysical Research Letters, vol. 31, no. 1, pp. 5, January 2004.

[6] Camps A, Vall-Llossera M, Villarino R, Reul N, Chapron B, Corbella I, Duffo N, Torres F, Miranda JJ, Sabia R, Monerris A, Rodriguez R, "The Emissivity of Foam-Covered Water Surface at L-Band: Theoretical Modeling and Experimental Results From the Frog 2003

Field Experiment", IEEE Trans. Geosci. Remote Sensing, vol. 43, issue 5, pp. 925-937, May 2005.

[7] Simon H. Yueh, Steve Dinardo, Alexander Fore, and Fuk Li, "Passive and Active L-Band Microwave Observations and Modeling of Ocean Surface Winds", IEEE Trans. Geosci. And Remote Sensing, Vol. 48, No. 8, pp. 3087-3100, August 2010.

[8] D.M. Le Vine, G.S.E. Lagerloef, R. Coloma, S. Yueh, and F. Pellerano, "Aquarius: An Instrument to Monitor Sea Surface Salinity from Space," IEEE Trans. Geosci. And Remote Sensing, Vol. 45, No. 7, 2040-2050, July 2007.

[9] Kraus, John D., Radio Astronomy, 2nd. ed., 1986, Cygnus-Quasar Books, Powell, Ohio.

[10] Thomas Meissner and Frank Wentz, The Complex Dielectric Constant of Pure and Sea Water From Microwave Satellite Observations, IEEE TGARS, vol. 42 (9), 2004, 1836 – 1849.

[11] Simon Yueh and J Chaubell, "Sea Surface Salinity and Wind Retrieval using Combined Passive and Active L-Band Microwave Observations", IEEE Trans. Geosci. Remote Sens., Vol. 50, No. 4, pp. 1022-1032, April 2012.

[12] Simon Yueh, Wenqing Tang, Alex Fore, Gregory Neumann, Akiko Hayashi, Adam Freedman, Julian Chaubell, and Gary Lagerloef, " L-band Passive and Active Microwave Geophysical Model Functions of Ocean Surface Winds and Applications to Aquarius Retrieval,", , to be submitted to IEEE TGRS, 2012.

[13] Yueh, S. H., "Estimates Of Faraday Rotation With Passive Microwave Polarimetry For Microwave Remote Sensing Of Earth Surfaces," IEEE Trans. Geosci. Remote Sensing, Vol. 38, No. 5, 2434-2438, September 2000.

[14] Burton, S. Garbow, Kenneth E. Hillstrom, Jorge J. More, Documentation for Minpack, Argonne National Laboratory, http://www.netlib.org/minpack/

[15] J. Figa-Saldaña, J.J.W. Wilson, E. Attema, R. Gelsthorpe, M.R. Drinkwater, and A. Stoffelen, The advanced scatterometer (ASCAT) on the meteorological operational (MetOp) platform: A follow on for European wind scatterometers, *Can. J. Remote Sensing*, Vol. 28, No. 3, pp. 404–412, 2002.

[16] Stoffelen A., "Toward the true near-surface wind speed, "Error modeling and calibration using triple collocation," J. Geophysical Research, Vol. 103, No. C4, pp. 7755-7766, April 15, 1998.

[17] Jur Vogelzang, Ad Stoffelen, Anton Verhoef, and Julia Figa-Saldaña, On the quality of high-resolution scatterometer winds, J. Geophysical Research, Vol. 116, C10033, doi:10.1029/2010JC006640, 2011.

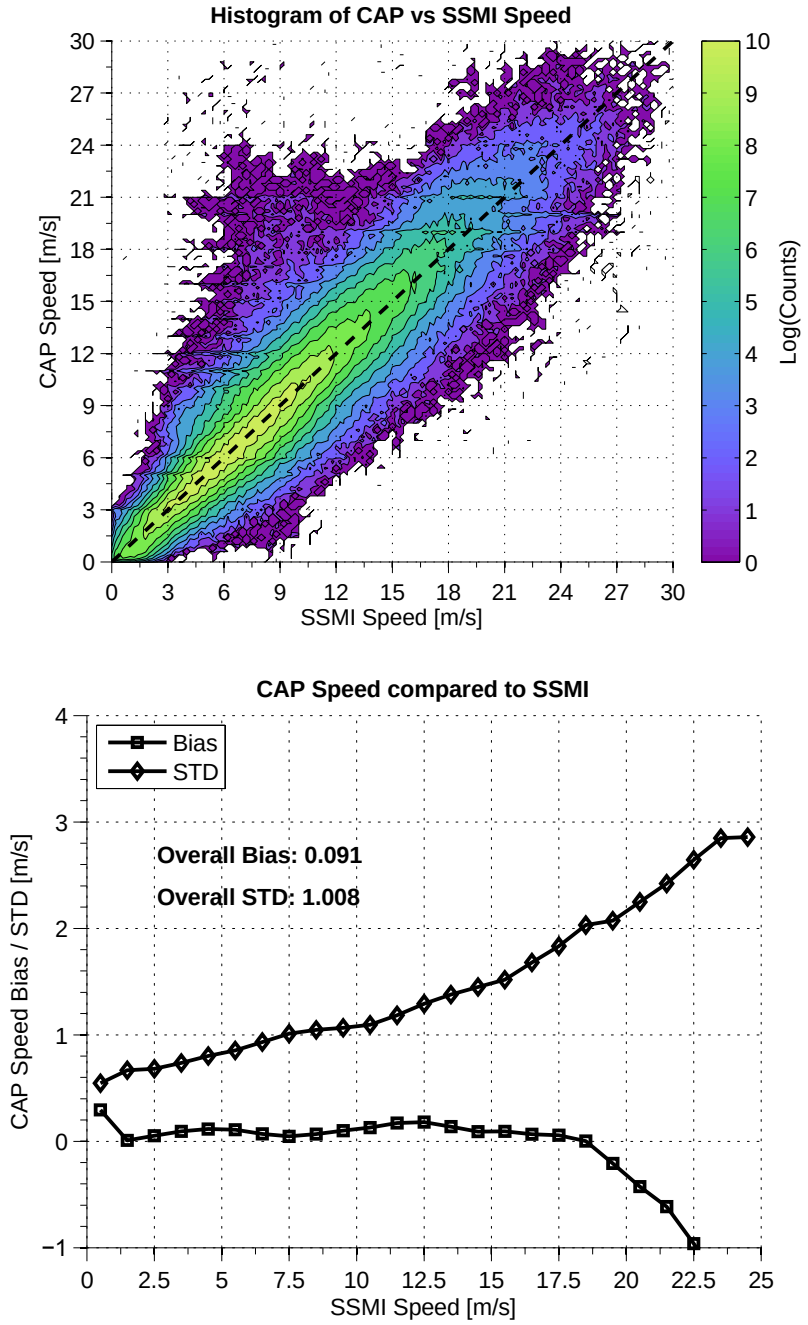

Figure 1. The wind speed retrievals from the CAP algorithm are compared with the SSM/I wind speed. The upper panel illustrates the scatter with respect to the SSM/I wind speed for retrievals from late August 2011 to December 2012. The bottom panel plots the bias and standard deviation of the differences with the SSM/I wind speeds.

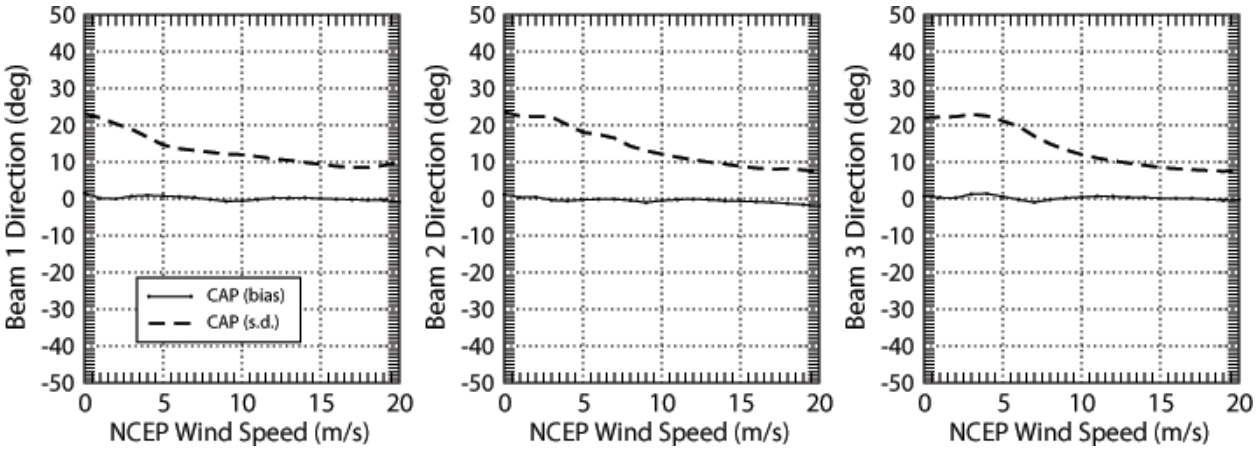

Figure 2. The wind direction retrievals from the CAP V2.0 algorithm are compared with the NCEP wind direction for the first four weeks in 2012. The left panel (beam 1), middle (beam 2) and right (beam 3) plot the bias and standard deviation of the differences with the NCEP wind direction.

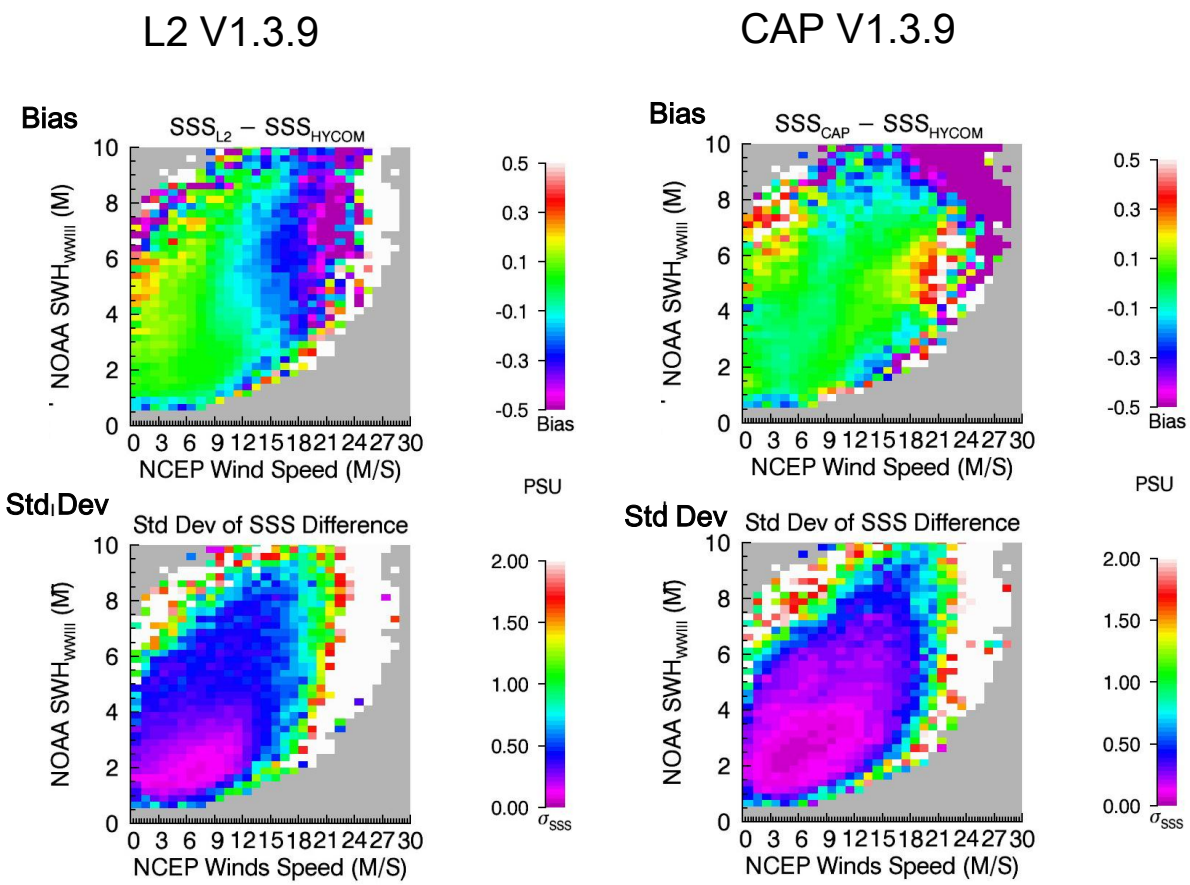

Figure 3. The monthly averaged SSS retrievals binned on 1x1 degree latitude and longitude grids are compared with the HYCOM salinity. The left panels plot the bias and standard deviation of the differences with respect to the HYCOM SSS for Aquarius v1.3.9 product in the 2-d SWH and wind speed space. The right panels are for the CAP V2.0 algorithm applied to the v1.3.9 data.

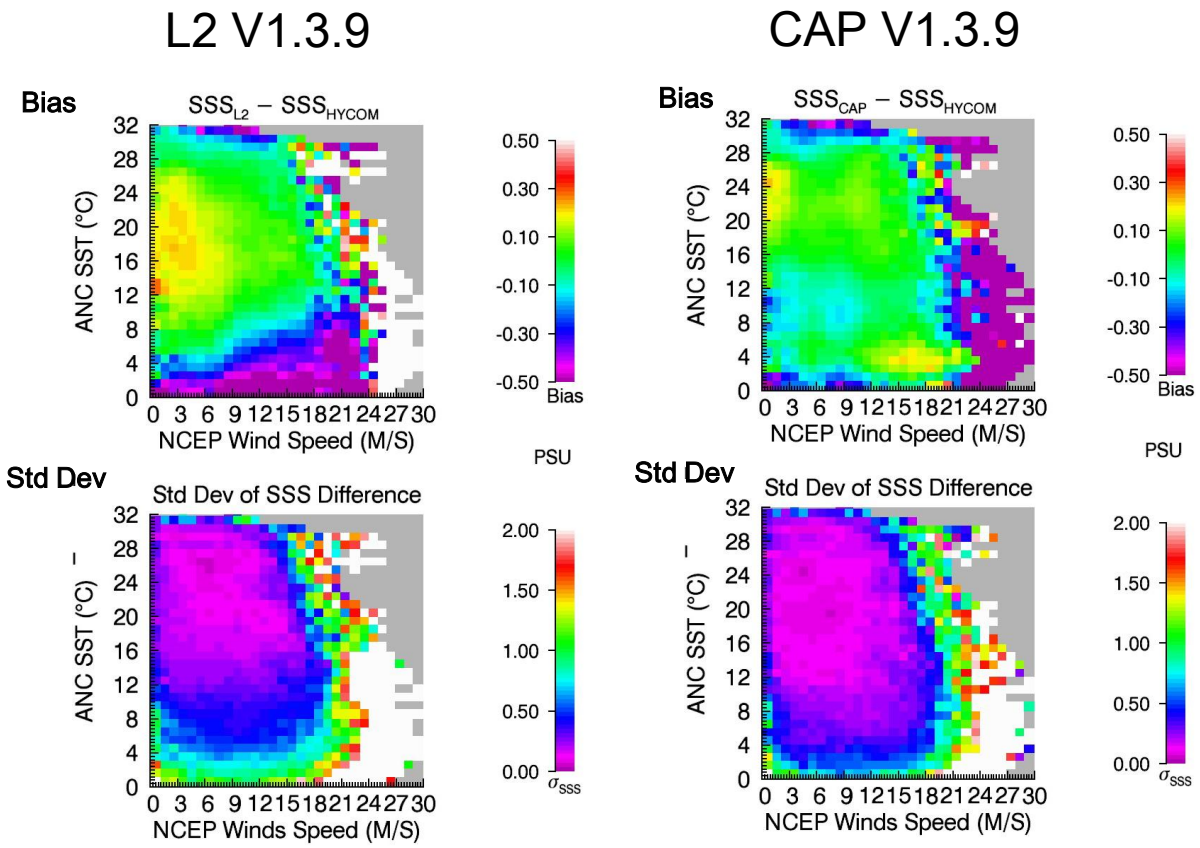

Figure 4. The monthly averaged SSS retrievals binned on 1x1 degree latitude and longitude grids are compared with the HYCOM salinity. The left panels plot the bias and standard deviation of the differences with respect to the HYCOM SSS for Aquarius v1.3.9 product in the 2-d SST and wind speed space. The right panels are for the CAP V2.0 algorithm applied to the v1.3.9 data.

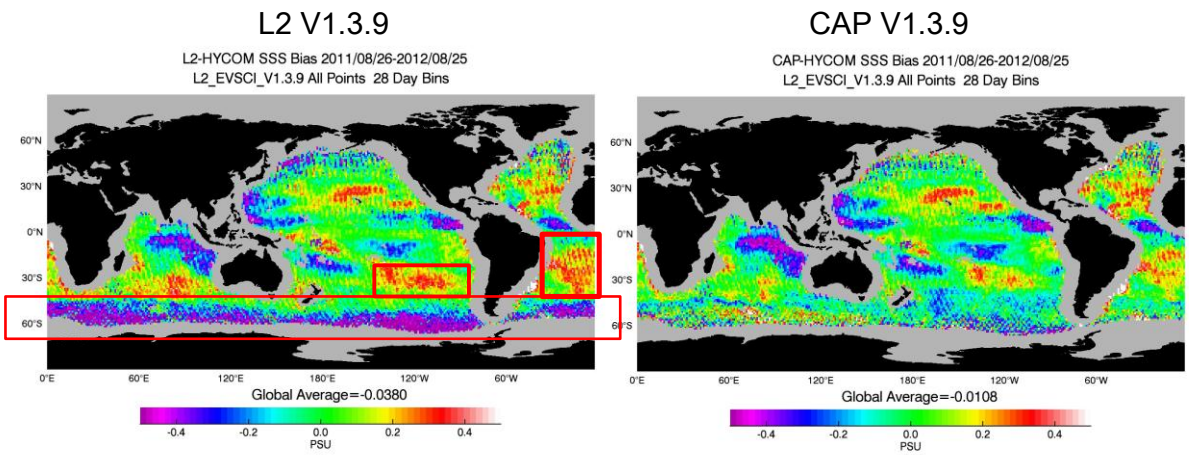

Figure 5. The monthly averaged SSS retrievals binned on 1x1 degree latitude and longitude grids are compared with the HYCOM salinity. The left panels plot the mean of the differences with respect to the HYCOM SSS for Aquarius v1.3.9 product on the latitude and longitude grids. The right panels are for the CAP V2.0 algorithm applied to the v1.3.9 data.

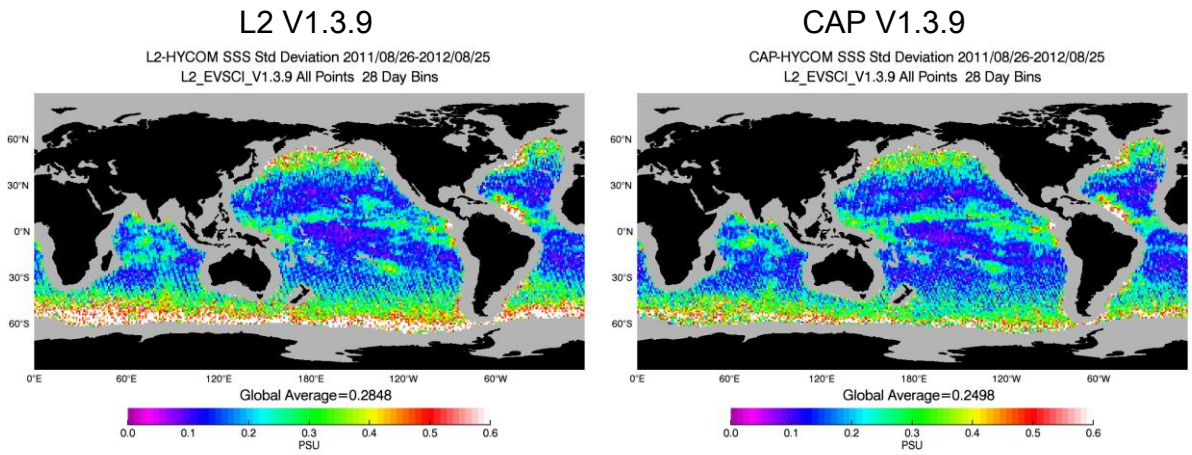

Figure 6. The monthly averaged SSS retrievals binned on 1x1 degree latitude and longitude grids are compared with the HYCOM salinity. The left panels plot the standard deviation of differences with respect to the HYCOM SSS for Aquarius v1.3.9 product on the latitude and longitude grids. The right panels are for the CAP V2.0 algorithm applied to the v1.3.9 data.

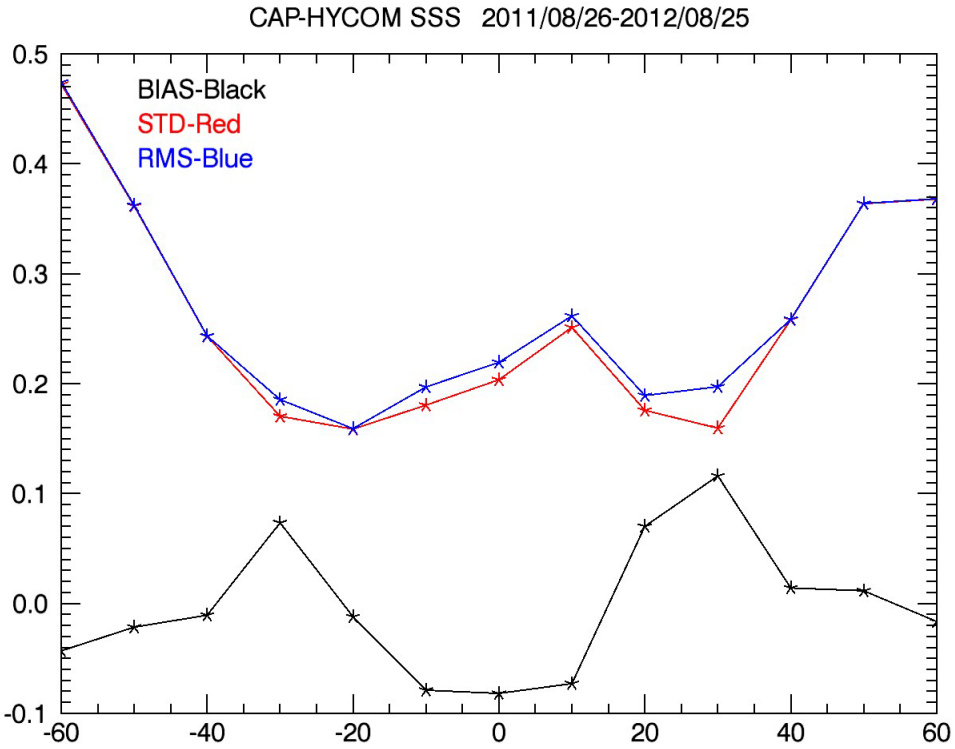

Figure 7. The monthly averaged SSS retrievals binned on 1x1 degree latitude and longitude grids are compared with the HYCOM salinity. The mean and standard deviation illustrated in Figs. 5 and 6 are averaged over 10 degrees in latitude.